Received 17 April 2021; revised 17 May 2021; accepted 20 May 2021. Date of publication 26 May 2021; date of current version 9 June 2021.

Digital Object Identifier 10.1109/OJAP.2021.3083932

4-Port MIMO Antenna Using Common Radiator on a Flexible Substrate for Sub-1GHz, Sub-6GHz 5G NR, and Wi-Fi 6 Applications

KUMUD RANJAN JHA [1] (Senior Member, IEEE), Z. A. PANDIT JIBRAN [1], CHITRA SINGH [2] (Member, IEEE), AND SATISH KUMAR SHARMA [3] (Senior Member, IEEE)

[1]School of Electronics and Communication Engineering, Shri Mata Vaishno Devi University, Katra 182320, India

[2]Center for the Advanced Studies, Dr. A. P. J. Abdul Kalam Technical University, Lucknow 226031, India

[3]Department of Electrical and Computer Engineering, San Diego State University, San Diego, CA 92182, USA

CORRESPONDING AUTHOR: K. R. JHA (e-mail: jhakr@rediffmail.com)

ABSTRACT In this paper, an angular symmetric, common radiator coplanar waveguide (CPW) fed four-port multiple-input-multiple-output (MIMO) antenna is designed on a $0.129\lambda_L^2$ RT Duroid ($\varepsilon_r = 3.0$, $\tan\delta = 0.001$) substrate where λ_L is the free space wavelength at the lowest operating frequency (f_L) of 0.6 GHz. The antenna has a −6 dB impedance bandwidth from 0.6-1.09 GHz, 2.6-3.4 GHz and 4.2-7.0 GHz to cover the emerging wireless communication bands. At the same time, it also has a −10 dB impedance bandwidth extending from 0.7-1.01 GHz, 2.6-3.18 GHz, 5.3-6.06 GHz, and 6.7-6.94 GHz. Design steps to enhance the operating bandwidth and the isolation in the sub-1GHz bands are presented. The antenna has a reasonable realized gain at the simulated and measured frequencies. It exhibits the pattern diversity which is useful for the MIMO implementation. The envelope correlation coefficient (ECC), Mean effective gain (MEG), and the channel capacity of the antenna have been computed from the measured results. In spite of the small circuit size at f_L, the ECC $\leq$ 0.50 over the entire band is observed. In addition to the existing communication applications, this antenna can find newer applications in the emerging 0.6-1.09 GHz band, sub-6GHz 5G near radio (NR), and Wi-Fi 6 communications.

INDEX TERMS 0.6 GHz, 4G, 5G, integrated antenna, pattern diversity, sub-7GHz.

I. INTRODUCTION

TO ENHANCE the wireless data transfer rate to meet the emerging requirements, the multiple-input-multiple-output (MIMO) system has been proved to be the backbone of the 4th generation (G) and beyond wireless communication systems [1]. A number of MIMO antennas have been developed for the high data rate transmission where compact printed circuit board (PCB) antennas are commonly designed [2]. To meet the space constraints in the sub-1 GHz communication bands, two antenna elements have widely been used to enhance the channel capacity [3]–[4]. Since, the channel capacity can be significantly improved by increasing the number of antenna elements; a four port antenna designed using multi-object optimization technique to operate in 2.5-2.75 GHz and 3.35-3.85-GHz band is reported in [5]. Similarly, a quad-element antenna by replicating the individual element, with a separated ground plane for each element operating above 2.6 GHz with the isolation (I) $\geq$ 14 dB is reported in [6]. Using the self-curing decoupling technique, four port narrow band monopole MIMO antenna with the improved isolation but only in a very narrow band around 2.14 GHz is presented in [7]. A compact four element MIMO antenna designed using inverted L-shaped monopole operating in 2.7-4.94 GHz range with $I \geq$ 10 dB between collinear ports is reported in [8]. It is worthy to mention that the isolation improvement between the collinear ports is challenging and the problem aggravates with the reduction in operating frequency. Using the lumped elements, the isolation can be improved and a four port antenna to operate in 3.4-3.6 GHz band is reported in [9]. However, at such

a high frequency, isolation is only 11.6 dB. The electromagnetic bandgap (EBG) structure has been placed in the middle of the four widely separated monopole antennas to reduce the mutual coupling to 17 dB operating above 3 GHz in [10]. A four-element half–circle shaped printed MIMO antenna to operate above 2.4 GHz with the envelope correlation coefficient (ECC) = 0.3 is reported in [11]. The pre-matched Eigen mode antenna with polarization and pattern diversity to operate in 2-6 GHz range is reported in [12]. It uses the hybrid couplers to change the phase which increases the design complexity and the profile. Using the split-ring resonator (SRR), a four-element antenna operating in 1.95-2.5 GHz band with an $I \geq 17$ dB is reported in [13]. However, the antenna uses four separate ground planes. For the access point applications, with four squinted beams, an antenna operating in 1.8-2.9 GHz band is reported in [14]. In another approach, the multi-port 4G MIMO system operating above 2.4 GHz has been integrated to a 28.0 GHz 5G band antenna [15]. Authors integrated the 4-port 4G MIMO antenna operating above 1.9 GHz with impedance bandwidth (IBW) $= -6$ dB and $I \geq 12$ dB to 5G antenna systems in [16]. The defected ground structure has also been used to increase $I \geq 17$ dB of a four port antenna operating above 3.5 GHz in [17].

To simplify the fabrication, in place of multiple radiating elements, a single radiating element with the multiple ports has also been developed [18]–[19]. Although simple in design, they operate above 2.0 GHz.

Interestingly, with a thrust to miniaturize the profile and improve the isolation, the majority of the 04 port antennas have been designed to operate above 2.0 GHz only. With the decrease in the operating frequency, the coupling between the ports increases and it becomes a challenging task to maintain a decent isolation [18]–[19]. Similarly, using the common ground and the coplanar waveguide (CPW) feeding, the MIMO antennas for the wireless communications are reported in [20]. Although, the antenna has the advantage of series integration and the fabrication simplicity, operates above 3.0 GHz, only.

Based on these criteria, a distinction between sub 1-GHz and above 1-GHz antennas can be inferred from [21]. Owing to the ground plane size with respect to the operating frequencies, for the sub-1GHz antennas, IBW $= -6$ dB and $I \geq 10$ dB have been used in [21]–[22]. Seldom, a multiport antenna to operate below 1.0 GHz has been designed [23]. However, for the 4G and beyond, the sub-1GHz communication bands are important [2]–[3] which requires attention.

In the recent years, the sub-1GHz long term evolution (LTE) is considered to be the potential candidate for high data rate communication and its application scenarios are described in [24]–[28]. However, the MIMO implementation which is the key technological advancement of the LTE band communication is challenging in sub-1GHz [29].

To meet the exponentially growing data rate requirements for the Internet of Things (IoT), the use of the mid-band frequency spectrum, sub-6GHz 5G near radio (NR), and the IEEE 802.11ax or Wi-Fi 6 standard for the next generation communication systems is proposed [30]–[34]. The Wi-Fi 6 band is to be available in four sub bands 5.925-6.425GHz, 6.425-6.525GHz, 6.525-6.875 GHz and 6.875-7.125 GHz extending over 5.925-7.1725 GHz frequencies [33]. Further, for the high data rate transmission using multiple standards, the co-existence of the LTE band with the Wi-Fi bands is suggested in [35]. It indicates that in MIMO implementation, the sub-1GHz LTE band should be integrated to the 5G NR and Wi-Fi-6 standard for the future high speed IoT and Wi-Fi applications.

Thus, to meet the sub-1GHz LTE band, sub-6GHz 5G NR, and the Wi-Fi 6 wireless communication requirements, the CPW fed a 04 port common radiating element antenna in MIMO implementation is presented here. The paper has the following new antenna contributions with unique features:

1) The antenna operates over the upcoming communication bands in 0.6-1 GHz, sub-6GHz 5G NR, and Wi-Fi 6 communication bands in addition to the mid band ($\sim$ 3GHz).
2) The multi-band circular printed monopole antenna is designed using the characteristic mode analysis (CMA) and a design curve to find the suitable dimensions, is presented.
3) Steps to enhance the operating bandwidth of this antenna using stubs in the sub-1GHz band are presented.
4) The stub loaded antenna has the omnidirectional radiation pattern and it offers the pattern diversity suitable for the MIMO implementation.
5) It is a 4-port antenna topology with the co-surfaced ground plane which may lead to the design of the conformal and 3-D MIMO antennas in the future.

Section II discusses the design of a circular printed monopole antenna using the characteristic mode analysis (CMA). Section III discusses the bandwidth enhancement steps. In Section IV, a 04-port CPW fed common radiator antenna is proposed. In Section V the isolation improvement mechanism is shown. In Section VI, the radiation characteristics of the antenna are shown. Section VII shows the measured results. In Section VIII, the MIMO characteristic is verified. In Section IX, the state- of- the-art comparison is made. Section X concludes the work.

II. SINGLE ELEMENT RADIATING PATH DESIGN

A. HISTORICAL PERSPECTIVE OF CIRCULAR MONOPOLE ANTENNA

The circular printed monopole antenna has extensively been studied in the past [36]–[50]. In majority of cases, using the parametric study, these antennas are designed for the ultra-wideband (UWB) applications to operate above 2.0 GHz, where wide bandwidth is obtained by controlling overall size of the substrate, radius of the printed monopole, and feed length reduction obtained by increasing the ground plane size. The parametric study has extensively been used to

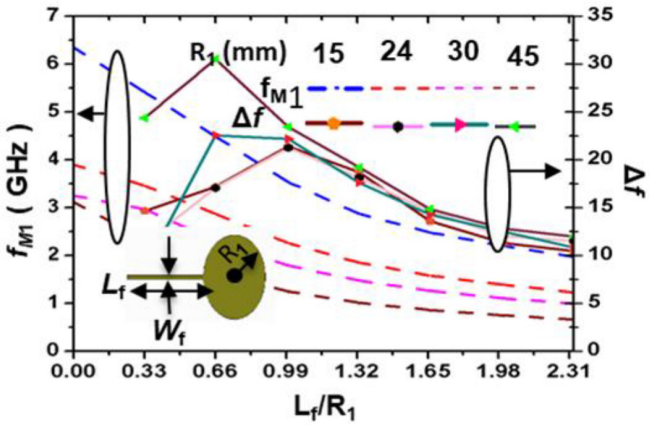

FIGURE 1. CMA of a circular printed monople and its resoanting behavior.

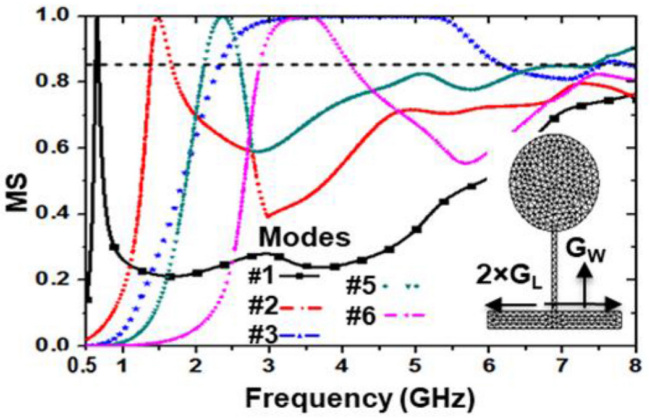

FIGURE 2. Modal significance of the antenna with meshing view.

lower the operating frequency (f_L) which is sensitive to these parameters. Nevertheless, it has also been used for the multiband applications where modification in the ground plane or in the printed monopole itself, is inevitable [51]–[52]. The ground plane size and the asymmetric modification made in it, have the limited use in the flexible MIMO implementation. The larger ground plane can increase the mutual coupling and reduce the isolation. Similarly, the asymmetric modification in the ground plane can lead to the asymmetric surface current distribution to affect the operating bandwidth and the radiation characteristics when used in MIMO implementation.

For the quest of larger operating bandwidth and to use it in the MIMO implementation in sub-1GHz band, a single circular printed monopole antenna as a basic building block using CMA technique is analyzed in the next section. The analysis reveals the effect of the feed length and monopole antenna radius on the operating frequency and percentage change in the frequency with respect to (w.r.t.) the change in ratio of the feed length to radius.

B. CHARACTERISTIC MODE ANALYSIS OF CIRCULAR PRINTED MONOPOLE

From the interpretation of the modal significance (MS), CMA has widely been used in the antenna placement, the bandwidth enhancement, and the decoupling [53]–[56]. Here, it is used to design a multiband antenna to meet 0.6-1.0 GHz and the higher band communication requirements. A planar circular printed monopole with the feed-line (L_f) is shown as the inset in Fig. 1. In general, the feed-line width (W_f) is smaller than the wavelength corresponding to the first modal resonance frequency (f_{M1}) and thus the effect of L_f on f_{M1} and the relative percentage change in the resonance frequency (Δf) with respect to L_f for four different cases are shown in Fig. 1. It shows that by suitably selecting the L_f/R_1 where R_1 is the radius of the printed circular monopole, f_{M1} and Δf can be controlled to meet the intended design requirements. With $L_f = 0$, the circular printed monopole resonates in its fundamental mode. When keeping R_1 fixed, L_f is increased, the f_{M1} is decreased. The same characteristic is observed for the all four cases of the R_1 under the investigation as shown in Fig. 1. Thus, for the given R_1, by increasing L_f/R_1, the f_{M1} can be reduced. Secondly, the effect of L_f/R_1 on the change in the Δf is shown. For the larger L_f/R_1, Δf converges around 10%. It is also noticed that to operate at a specific f_{M1}, for the larger circular monopole radius, a smaller feed-length is required. Contrary to this, when the monopole radius is reduced, the feed-length must be increased. Thus, this figure gives an extra degree of freedom in selecting R_1 and L_f to design a compact circular printed monopole antenna.

Based on the above design guideline, a CPW fed antenna with $R_1 = 30$ mm is selected. Its f_{M1} ($L_f/R_1 = 0$) is close to 3 GHz which is lowered by using a feed with $L_f = 60$ mm ($L_f/R_1 = 2$). For $L_f/R_1 = 2$, f_{M1} is close to 1.01 GHz which can be further lowered by additional metallic strip loading. As shown in Fig. 2, by adding the metallic sheet ($G_L \times G_W$), in addition to f_{M1}, f_{MN} where $N = 1, 2, 3\cdots$ can also be controlled to obtain the multimodal resonance frequencies and the bandwidth. In Fig. 2, G_L and G_W are 45 mm, and 10 mm, respectively. Five modal frequencies excluding Mode#4 are shown. Mode #4 has MS lesser than 0.5 and thus can't be considered for the good resonating structure. From this figure, it is noticed that these modes satisfied the MS $\geq$ 0.86 over the wide frequency band where antenna can be designed with a -6 dB impedance bandwidth criterion. Secondly, the f_{M1} is 0.643 GHz which can be exploited to achieve a large bandwidth in the sub-1 GHz band.

After obtaining the lower band MS, the metallic strip $G_W \times 2G_L$ is converted into the ground plane and is modified by cutting a slit (g) to accommodate the SMA connector. Considering a practical antenna, it is placed on a 1.52mm thick flexible Rogers RO3003 ($\varepsilon_r = 3.0$, $\tan\delta = 0.001$) substrate. Since, the resonator and ground plane are co-surfaced, the downward shift in the resonating frequency is very less because the effective permittivity is close to 1.0 [57]. The antenna element, surface current density (Js)

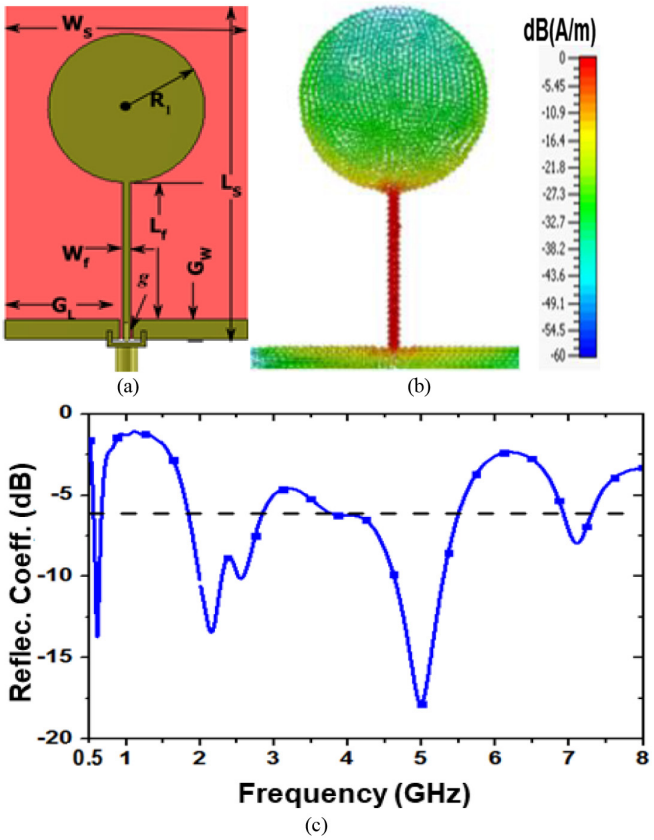

FIGURE 3. A simple antenna (a) topology (b) its characteristic mode *Js* and (c) Reflec. Coeff. magnitude in dB response.

TABLE 1. Design parameters of the proposed antenna.

Parameters	G_1	G_2	G_3	S_1	S_2	S_3	S_4	S_5	S_6	S_7
Value (mm^2)	6.25 × 3.5	6.0 × 3.9	5.5 × 2.3	42.5 × 5	20 × 2.7	15.3 × 7 ×2.7	7.1 × 3.1	11 × 2.5	28 × 2.5	28 × 2.7
Parameters	L_S	W_S	R_1	L_f	W_f	G_L	G_W	g	g_1	L_P
Value (mm)	130	90	29	53	2.9	42.5	7.4	1.04	0.5	8.2

at $f_{M1} = 0.643$ GHz, and the reflection coefficient (Reflec. Coeff.) of the antenna are shown in Fig. 3(a-c), respectively. The final antenna design parameters (R_1, G_L, G_W) are given in Table 1.

Comparing Fig. 3(c) with Fig. 2, it can be observed that the first resonance frequency ($f_{M1} = 0.643$ GHz, Fig. 2) is shifted to 0.605 GHz [Fig. 3(c)], which is due to the substrate effect and g. Secondly, corresponding to the Mode#2 and Mode#3, as shown in Fig. 2, the antenna resonates near 2.0 and 2.5 GHz [Fig. 3(c)]. Further, there is wide impedance bandwidth between 3.5-5.5 GHz [Fig. 3(c)] corresponding to Mode #3 (Fig. 2). Additionally, it is noticed that Modes # 3, #5, and #6 converges near 7.0 GHz in Fig. 2. Corresponding to this, the antenna resonates near 7.0 GHz in Fig. 3(c). Thus, a one to one correspondence between the CMA based modal resonance frequencies and the achievable resonating bands for a practical antenna can be established.

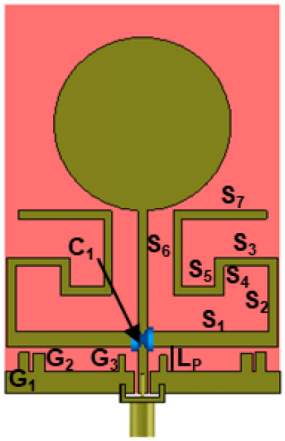

FIGURE 4. Stub loaded circular printed monopole (parameters in Table 1).

III. STEPS TO ENHANCE OPERATING BANDWIDTH

As shown in Fig. 3(c), the antenna resonates at a very low frequency (0.605GHz) where it has a 33% fractional bandwidth (FBW). The resonance frequency and operating bandwidth can be modified by the stub loading [58]. A stub loaded modified antenna is shown in Fig. 4. The bandwidth enhancement method is discussed in the subsequent paragraphs.

A. EFFECT OF GROUND PLANE STUBS

To enhance the operating bandwidth, the impedance matching level of the antenna is enhanced by loading the ground plane by stubs G_1, G_2, and G_3 as shown in Fig. 4 whose dimensions are given in Table 1. The position (distance between $G_1 - G_2 = 1.0$mm, $G_2 - G_3 = 24.1$mm) and the dimensions are parametrically studied. The effect of the stub loading is shown in Fig. 5(a) where they impact on the real (Z(Re)) and imaginary (Z(Im)) part of the impedance. By adding $G_1 - G_3$ to the small ground plane ($G_W = 7.4$mm), the inductance is increased. Although, it does not significantly contribute to the lower frequency (f) band but in the 4.0 GHz $\leq f \leq$ 6.5GHz range, it increases the Z(Im) to improve the impedance matching by reducing the capacitive effect of the printed monopole. Consequently, Z(Re) also changes. Further, the comparison of the reflection coefficient (Reflec. Coeff.) magnitude with and without $G_1 - G_3$ is shown in Fig. 5(b). It shows that by increasing the Z(Im), the -6 dB impedance matching level above 2.9 GHz has been improved over the wide range.

B. EFFECT OF STUBS LOADING

Due to the inductive effect of $G_1 - G_3$, impedance matching level at $f \geq 1.8$ GHz has significantly improved. However, it is not an attractive solution for the sub-1GHz band and thus, the antenna is symmetrically loaded with $S_1 - S_7$. The cause of stub loading can be interpreted from the surface current density (Js) on the radiator at $f_{M1} = 0.643$GHz which has been obtained using CMA [Fig. 3(b)]. At this frequency, the feed-line has maximum Js which can be

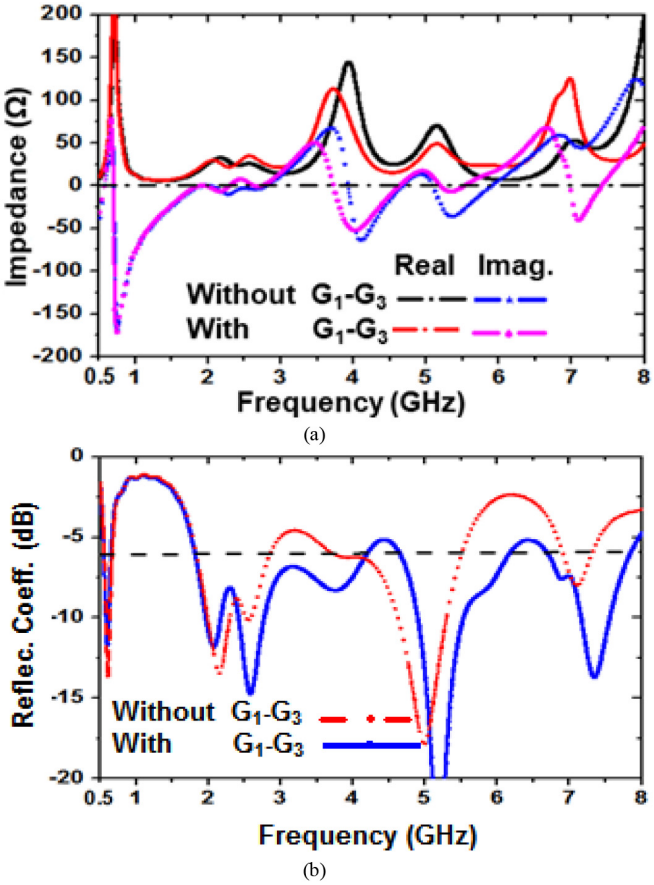

FIGURE 5. Effect of ground stubs on (a) impedance and (b) S_{11} magnitude.

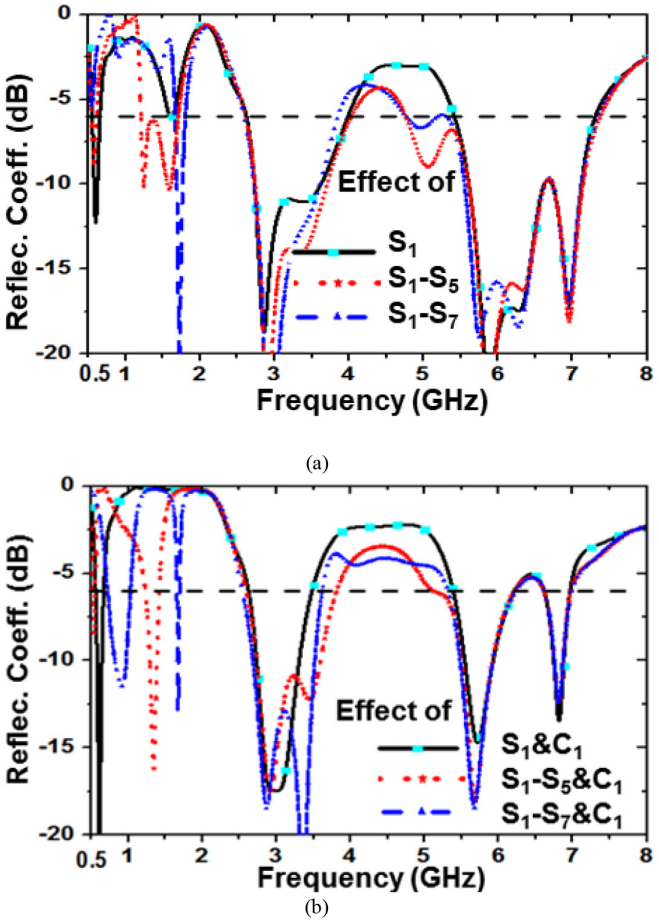

FIGURE 6. Effect of the (a) stubs and (b) stubs with C_1 on bandwidth.

suitably coupled to stubs to increase the bandwidth. The effect of the stub loading is shown in Fig. 6(a). To improve the legibility, Reflec. Coeff. (dB) for the total stub length $(L) = S_1$, $L = S_1 + \cdots + S_5$, and $L = S_1 + \cdots + S_7$ when stubs are cascaded, is shown. The symmetrically loaded stubs form a dipole which possesses the omnidirectional radiation characteristics in one of the radiation plane. As shown in Fig. 4, they are coupled to the main feed-line via capacitances $(C_1) = 100$pF. The value of C_1 is obtained by the parametric study which is not shown here for the sake of brevity. The effect of $C_1 = 100$ pF on the operating bandwidth in three cases, (i) C_1 with S_1 only, (ii) C_1 with $S_1 + \cdots + S_5$, and (iii) C_1 with $S_1 + \cdots + S_7$, are shown in Fig. 6(b). For the last case, in sub-1GHz range, the antenna has a 0.71-1.03 GHz wide -6dB impedance bandwidth. It also has a -6dB bandwidth from 1.65-1.70 GHz, 2.5-3.6 GHz, 5.3-6.2 GHz and 6.63-6.98 GHz. When capacitive elements are connected between the stubs and the feed-line, it lowers the quality factor over the wide frequency range to improve the bandwidth and thus the use of the stubs with capacitance in the CPW fed antenna design is justified. The antenna also offers a -10dB impedance bandwidth from 0.81GHz-0.97 GHz, 1.66-1.68 GHz, 2.67GHz-3.53 GHz, 5.4GHz-5.95 GHz, and 6.73-6.88 GHz. Thus, in this type of the antenna, the stub loading along with the lumped capacitance can be used to increase the operating bandwidth in sub-1GHz range.

IV. FOUR PORT MIMO ANTENNA DESIGN

In this section, using the single circular printed monopole antenna as shown in Fig. 4, a 04 port antenna with the common radiator has been designed. In Section II, the single circular printed monopole has been exhaustively investigated for its one to one correspondence to the MS of the CMA. In Section III, the operating bandwidth has been increased in sub-1GHz band. Thus, maintaining the approximately same operating bandwidth as shown in Fig. 6, in this section, a common radiator but rotationally symmetric, a 04 port MIMO antenna which is rotated about the center of the circular monopole, is presented.

Due to the rotational symmetry about the center of the monopole, the antennas as shown in Fig. 4 can be converted into a multi-port MIMO antenna system with the common circular radiating monopole. A four-port antenna designed using this method is shown in Fig. 7(a). The substrate side lengths and the total area of the antenna are $2 \times W_s$ (180mm), and $0.129\lambda_L^2$ where λ_L is the lowest frequency wavelength at 0.6GHz, respectively. The remaining design parameters are same as given in Table 1. In this topology, port pairs

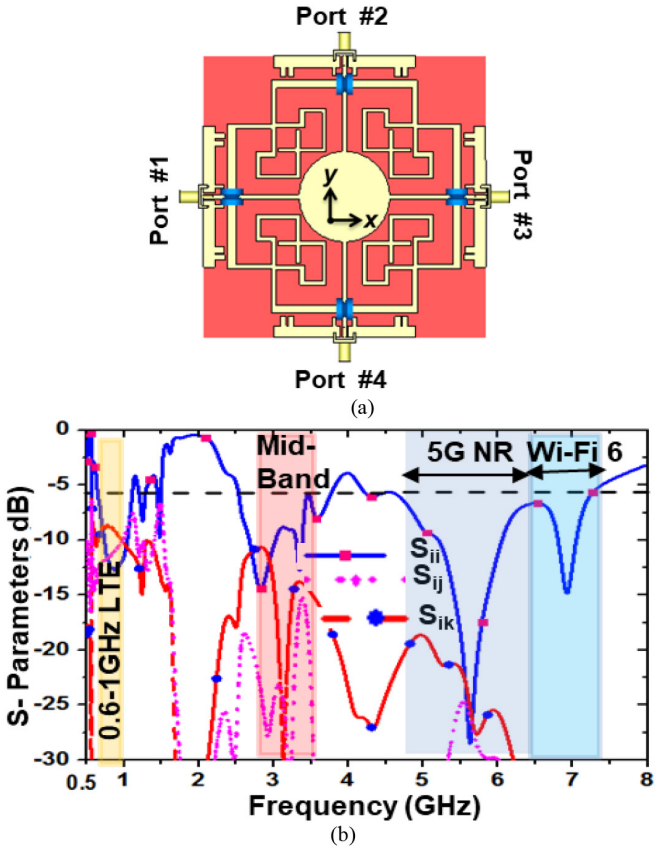

FIGURE 7. Four port (a) Antenna and (b) S-parameter (magnitudes).

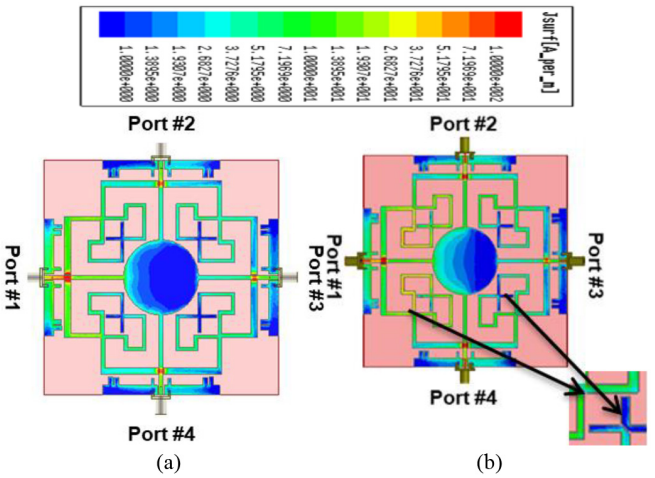

FIGURE 8. *Js* on the antenna when Port#1 excited and others are terminated in matched load (a) without slot and (b) with slot g_1.

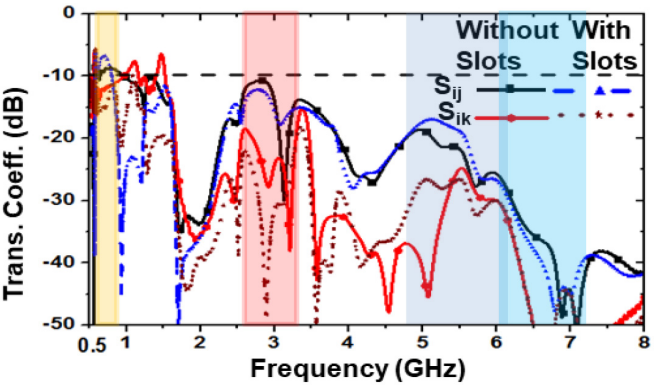

FIGURE 9. Effect of the slots in overlapping region on the Trans. Coeff. (magnitude) in the intended bands ($S_{ij} = S_{21}, S_{32}, S_{43}, S_{14}$ & $S_{ik} = S_{31}, S_{42}$).

Port#1-2, Port#2-3, Port#3-4 and port#1-4 are the orthogonal ports. Similarly, port pairs Port#1-3 and Port#2-4 are the collinear ports. The S-parameter (dB) at these ports in the intended frequency bands are shown in Fig. 7(b). In this figure and hereafter in the paper, S_{ii}, $S_{ij,}$ and S_{ik} represent the Reflec. Coeff. (dB) at i^{th} ports, the transmission coefficient (Trans. Coeff.) between orthogonal ports, and the Trans. Coeff. between collinear ports, respectively. Even with the small ground plane width ($G_W = 7.4$mm), the structure shows a wide -6 dB bandwidth extending from 0.65-1.1 GHz, 2.50-3.78 GHz, and 4.2-7.2 GHz. The second band has shifted from 1.65-1.70 GHz to 1.44-1.49 GHz and the impedance matching level has reduced. The antenna also has a -10dB bandwidth from 0.69-1.01 GHz, 2.64-3.17 GHz, 5.3-6.08 GHz, and 6.73-6.95 GHz, in the simulated frequency range. In the sub-1GHz band, due to the proximity of the ports in comparison to the operating wavelength, the isolation deteriorates and $I > 10$dB among ports is a reasonable choice [21]–[23]. However, in the present case, it is 8.6dB between the two orthogonal ports. Similarly, the isolation between two collinear ports is better than 7.5 dB and its lowest value occurs at 1.1 GHz.

V. ISOLATION IMPROVEMENT

Isolation in the MIMO antennas depends on the port separation and it is challenging to improve with the decrease in the operating frequency [29]. To meet this challenge and to maintain a decent isolation over a wide operating band 0.6-1GHz for a common radiator antenna, a new technique is proposed.

Surface current density (J_s) on surface of the metallic radiator at 0.8 GHz of the four port antenna when Port #1 is excited and other ports are matched terminated to 50Ω is presented in Fig. 8(a). It shows majority of the leakage current through the overlapping regions of the stubs. The leakage through the common radiator is respectively low. Thus, overlapping reasons of the different antennas are separated by slots (g_1 as given in Table 1) of width 0.5mm each. Now, J_s is localized on the strips and makes the path from one port to other through the common radiator as shown in Fig. 8(b). The effect of these two cases on the Trans. Coeff. (magnitude) is shown in Fig. 9. When these strips are overlapping, in sub-1GHz band, the 4-port antenna has a wide -6dB impedance bandwidth in 0.65-1.1 GHz range. However, when slot is created, it reduces to 0.62-0.75 GHz but the impedance matching level is improved. Further, the isolation between orthogonal ports is reduced to 5dB. The

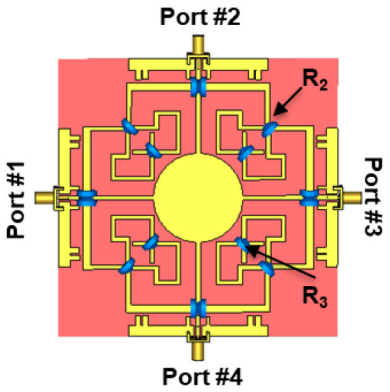

FIGURE 10. Proposed four ports antenna in MIMO implementation.

collinear port isolation remains unaffected and its minimum value is 10dB in the operating band.

It is important to note that when a narrow slot ($g_1 = 0.5$mm, Fig. 8(b)) is created, although total length of stubs $L = S1 + \cdots + S7$ has insignificantly changed; the quality factor has increased to reduce the operating bandwidth as shown in Fig. 11(a) (dotted line). Thus, it is intuitive to restively load the slot to lower the quality factor. Finally, after the parametric study, resistances $R_2 = R_3 = 60\Omega$ are placed across these slots. The proposed final antenna structure is shown in Fig. 10. The Reflec. Coeff. and Trans. Coeff. (magnitude in dB) of the antennas are shown in Fig. 11(a-b), respectively. Finally, due to the resistance loading, apart from the isolation improvement in the lower band, the -6dB bandwidth extends from 0.60-1.10 GHz which is higher than the previous two cases. However, due to it, the second band near 1.5GHz has detuned and shifted upward which can be tuned by improving the impedance matching level but it is not addressed here as it falls outside the intended application in the present paper. At high frequency, except a band notch around 4.0 GHz; the band extends from 2.5-7.2 GHz. The antenna also has a -10 dB bandwidth from 0.7-1.01 GHz, 2.6-3.16 GHz, 5.3-6.1 GHz, and 6.8-7.0 GHz. The isolation improvement over the wideband in the sub-1 GHz range is challenging which has been improved by the resistive loading at least by 3.0 dB to raise the collinear and orthogonal port isolation above 10 dB which is shown in Fig. 11(c).

From [36]–[51], it is understood that the bandwidth of the wideband printed monopole antennas are greatly influenced by the G_W and the L_f. To achieve the impedance matching over the UWB, these two parameters are increased and decreased, respectively. If we use the same conventional UWB antenna with the large G_W in the four-port MIMO implementation, due to the overlapping of the ground plane of the antenna elements, the isolation would be significantly reduced.

The design challenge of maintaining very low $f_L = 0.6$GHz and the decent $I \geq 10$ dB can be addressed by using the narrow stubs in conjunction with the capacitances and the resistances. Thus, it justifies the design of the stub loaded 4-port antenna.

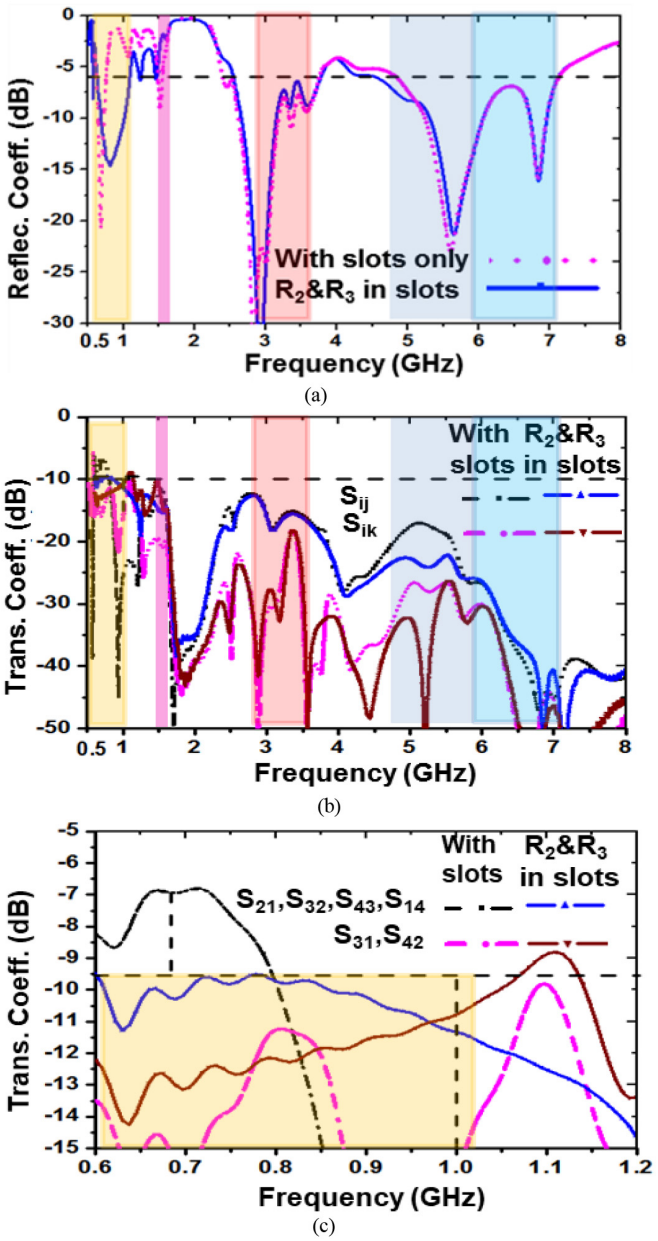

FIGURE 11. Effect of slot and resistance on (a) Reflection Coefficient and (b) Transmission Coefficient (Magnitude) in intended frequency bands ($S_{ij} = S_{21}$, S_{32}, S_{43}, S_{14} & $S_{ik} = S_{31}$, S_{42}) and (c) magnified view in sub-1.2GHz band.

VI. RADIATION CHARACTERISTICS

The simulated radiation and the antenna efficiency of two antennas; a single element, and a 04-port are shown in Fig. 12(a). The radiation efficiency of the single element is better than 98%. However, the total efficiency of the antenna depends on the impedance matching level. The radiation efficiency of the 04 port antenna is better than 70% over the intended frequency bands. However, the antenna efficiency drops to about 50% in sub-1GHz band.

To investigate its cause, the comparison of the antenna efficiency without and with the resistances (R_2&R_3) is made in Fig. 12 (b). It reveals a 5% drop in the antenna efficiency

VI. RADIATION CHARACTERISTICS

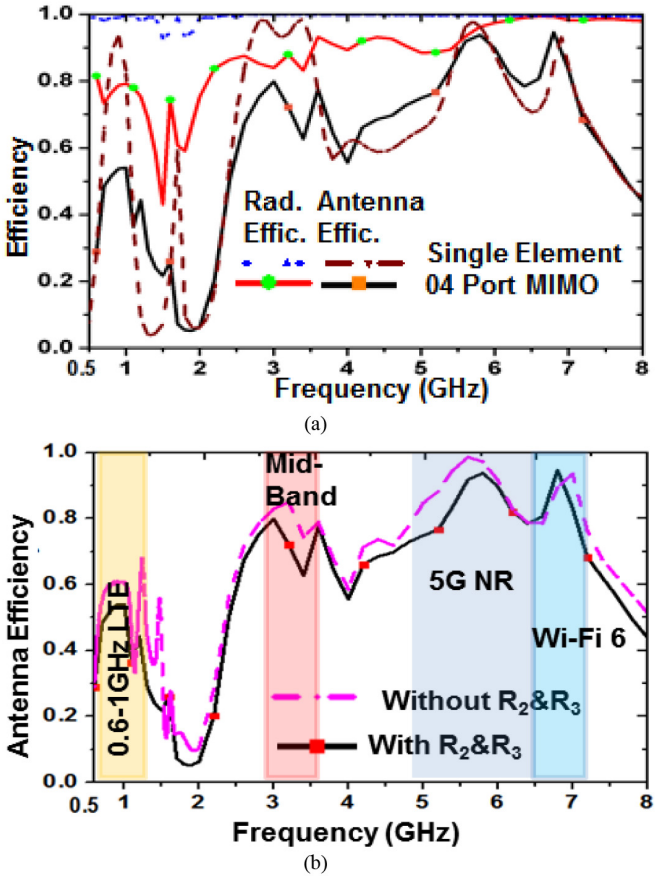

FIGURE 12. Efficiency of (a) two antennas and (b) with resistive loading.

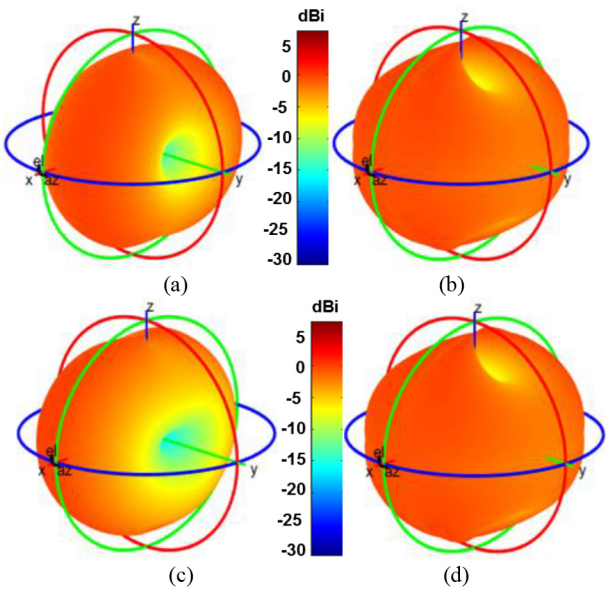

FIGURE 13. 3-D radiation pattern at Port (a) #1, (b) #2, (c) #3, (d)#4 at 0.8 GHz.

in sub 1-GHz band. However, the loss in the efficiency is less because it only perturbs the surface current near the overlapping region of the stubs.

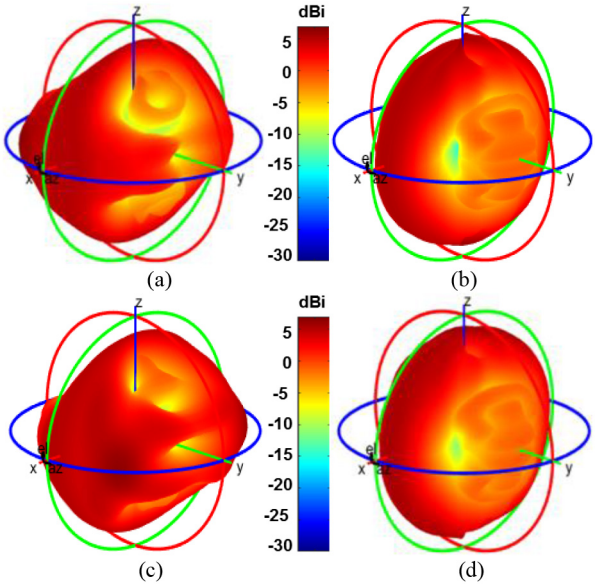

FIGURE 14. 3-D radiation pattern at Port (a)#1, (b)#2, (c)#3, (d)#4 at 5.8 GHz.

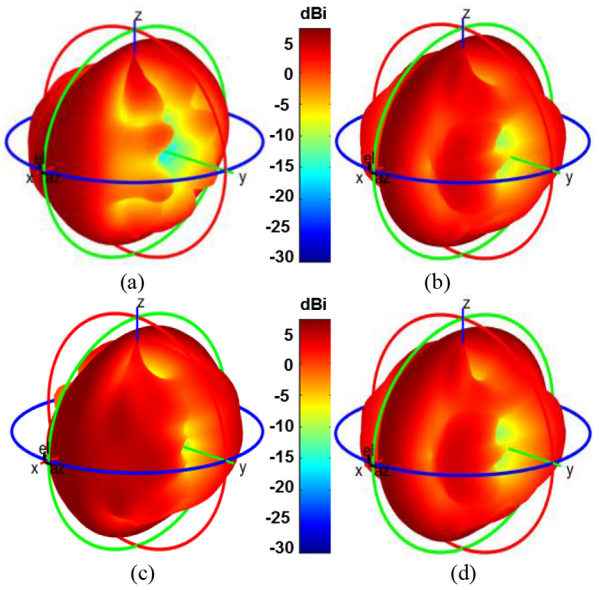

FIGURE 15. 3-D radiation pattern at Port (a) #1, (b) #2, (c) #3, (d)#4 at 7.0 GHz.

Due to the rotational symmetry of the stub loaded circular printed monopole, all four such antenna elements radiating in the orthogonal planes, are operating in the pattern diversity mode. The 3-D radiation pattern of all the four ports at 0.8 GHz, 5.8 GHz and 7.0 GHz are shown in Fig. 13, Fig. 14, and Fig. 15, respectively. Between two orthogonal planes, the null position of the antennas interchanges. Between collinear ports, the pattern shifts to left and right about the null-axis.

Secondly, at the 5.8 GHz, and 7.0 GHz, multiple lobes in the radiation pattern are visible which are due to the higher order mode generation. However, it can be observed that at all the frequencies, it shows a reasonable coverage.

TABLE 2. Simulated realized gain and directivity in various bands.

Electrical Characteristics	Frequency			
	0.8 GHz	3.0GHz	5.8GHz	7.0GHz
Realized Gain (dBi)	-0.05	4.4	6.9	5.0
Directivity (dBi)	2.82	5.4	7.2	5.4

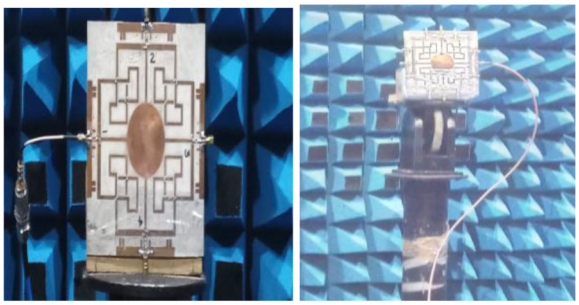

(a) (b)

FIGURE 16. Antenna (a) prototype and (b) in the anechoic chamber.

The electrical characteristics at different frequencies in the various communication bands are given in Table 2.

VII. EXPERIMENTAL VERIFICATION

The proposed antenna was fabricated using PCB Prototyping machine (EP42 Auto from EVERPRECESION) in Project Laboratory Shri Mata Vaishno Devi University (SMVDU), Katra, J&K, India and measured in the anechoic chamber at Antenna and Microwave Design Laboratory (AMD), SMVDU, Katra, J&K, India. The fabricated planar 4-port antenna is shown in Fig. 16.

The Reflec. Coeff (dB) at all ports of the antenna were measured. However, for the better view, along with the simulated results, the measured reflection coefficient at two orthogonal ports Port#1 and Port#2 are shown in Fig. 17(a). In sub-1GHz band, they are in good agreement with the simulated results. The band between 1.65-1.85 GHz is an artifact of the fabrication precision. Similarly, the bands towards higher end see differences compared to the simulated results due to fabrication.

The measured Trans. Coeff. (magnitude) between the orthogonal and collinear ports (S_{21} and S_{31}) are shown in Fig. 17(b). In sub-1GHz band, the measured transmission coefficient magnitudes are improved due to the cable losses. In general, in this band, and above 1.75 GHz bands, the measured isolation is better than 10dB and 20dB, respectively.

Due to the frequency limitation of the standard horn, the 2-D radiation patterns at all four ports of the antenna at 0.8 GHz, and 5.8 GHz have only been measured.

The measured normalized 2-D radiation pattern in the principle planes $\Phi = 0°$ and $\Phi = 90°$ at 0.8 GHz and 5.8 GHz are shown in Fig. 18 and Fig. 19, respectively.

The measured 2-D radiation pattern of the antennas shows a reasonable coverage area. However, at 5.8 GHz, the cross polarization level is relatively high due to the limited noise

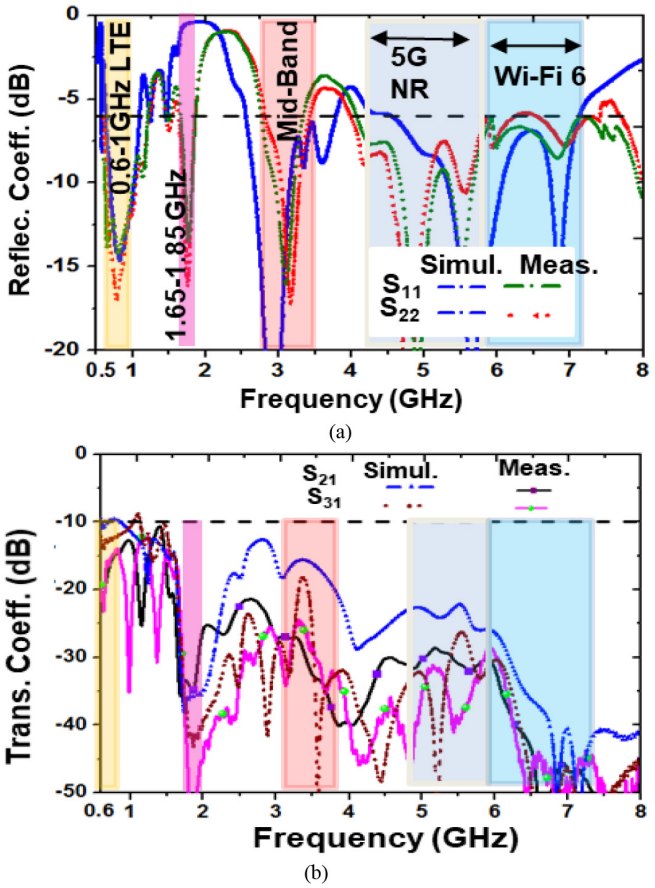

FIGURE 17. Measured (a) Reflection coefficient and (b) Transmission Coefficient of the planar antenna.

TABLE 3. Measured and simulated maximum realized gain in principle planes.

Port #	Realized Gain (dBi)			
	At 0.8 GHz		At 5.8 GHz	
	Simulated	Measured	Simulated	Measured
1	-0.05	-0.9	6.9	5.49
2		-0.61		5.37
3		-0.50		6.54
4		-0.80		5.53

floor of the anechoic chamber. Additionally, due to sagging of the substrate under the weight of the cable connectors, and due to the low mechanical support of the CPW fed SMA connectors in the chamber, some tolerable deviation in the measured radiation patterns is noticed. Nevertheless, it gives an insight that the antenna has a reasonable radiation characteristic.

The simulated and measured broadside peak realized gain in the principle planes ($\theta = 0°$, $\phi = 0°$ and $\theta = 0°$, $\phi = 90°$) at 0.8 GHz and 5.8 GHz are compared in Table 3 which shows a reasonable agreement. The small deviation between the simulated and measured realized gain is due to the change in the main beam directions. However, even with the small ground plane size, the realized gain is reasonably good.

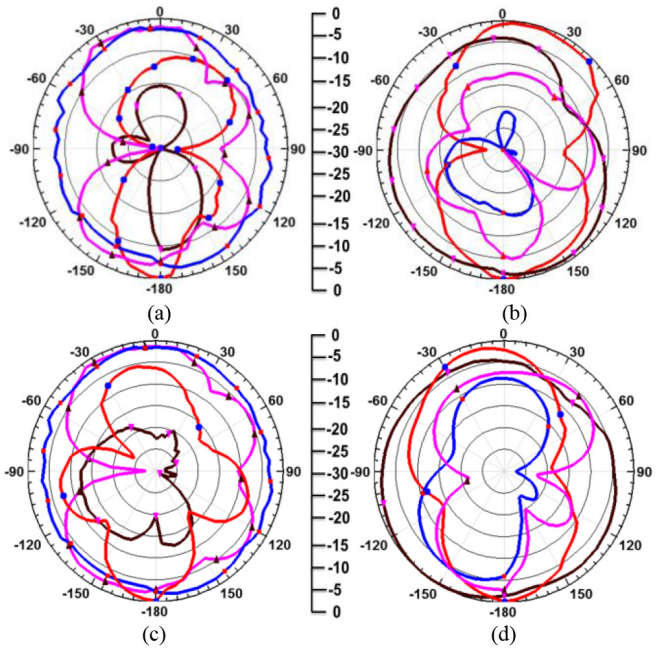

FIGURE 18. Measured 2-D radiation pattern (a) Port#1, (b) Port#2, (c) Port#3, and (d) Port#4 at 0.8 GHz (Gain Theta: Φ = 0° Φ = 90°, Gain Phi: Φ = 0° , Φ = 90°).

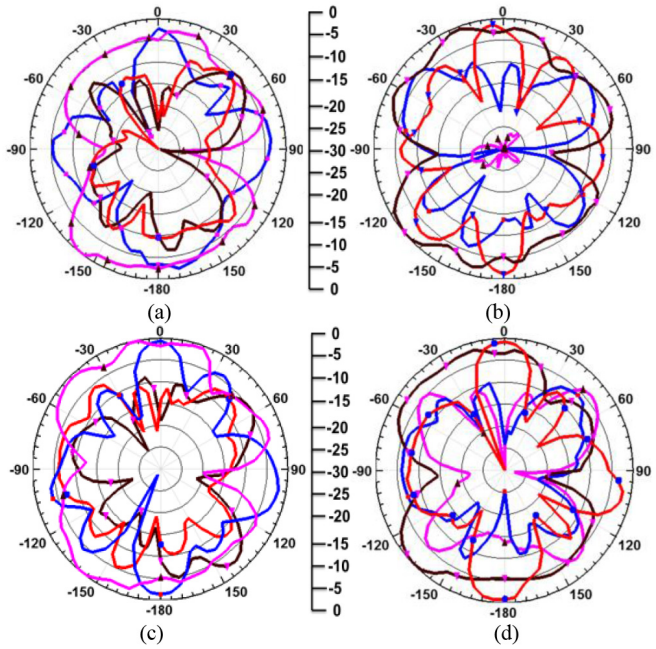

FIGURE 19. Measured 2-D radiation pattern (a) Port#1, (b) Port#2, (c) Port#3, and (d) Port#4 at 5.8 GHz (Gain Theta: Φ = 0° Φ = 90°, Gain Phi: Φ = 0° , Φ = 90°).

VIII. MIMO CHARACTERISTICS OF FOUR PORT ANTENNA

A. ENVELOPE CORRELATION COEFFICIENT (ECC)

The envelope correlation coefficient of the antenna is an important characteristic for the MIMO performance. The far-field radiation pattern based ECC is generally preferred to characterize this property [4]. However, it is a time consuming measurement technique. Since, the correlation among radiation patterns increases with the decrease in the circuit size with respect to the operating wavelength, hence to demonstrate the performance, using (1), we have computed the ECC from the measured 3-D radiation pattern at 0.8 GHz which describes the MIMO behavior of the antenna in sub-1GHz band [4]. In this equation, $\vec{G_i}(\theta, \phi)$ and $\vec{G_j}(\theta, \phi)$ are the gain pattern of the i^{th} and j^{th} antennas, respectively.

$$ECC = \frac{\left| \iint_{4\pi} \vec{G_i}(\theta, \phi) \bullet \vec{G_j}(\theta, \phi)^* \partial\Omega \right|^2}{\iint_{4\pi} \left| \vec{G_i}(\theta, \phi) \right|^2 \partial\Omega \iint_{4\pi} \left| \vec{G_j}(\theta, \phi) \right|^2 \partial\Omega} \quad (1)$$

The simulated and measured ECC at all four ports are summarized in Table 4. The ECC between orthogonal ports are very less but between the collinear ports, it increases. To understand the behavior of ECC over the entire frequency bands, the simulated ECC using two commercially available software CST Microwave Studio and Ansys HFSS is shown in Fig. 20. The comparison shows ECC $\leq$ 0.50 in the useful bands obtained in sub-1 GHz and above 2.5 GHz frequency range. The ECC between collinear ports are high and decreases with increase in the operating frequency because the electrical distances between ports increases with the increase in the operating frequency.

TABLE 4. Measured ECC pattern at 800MHz.

ECC	Port #1-2	Port #1-3	Port #1-4	Port #2-3	Port #2-4	Port #3-4
Simulated	0.01	0.28	0.01	0.01	0.28	0.01
From Measured E-Field	0.09	0.22	0.06	0.07	0.23	0.05

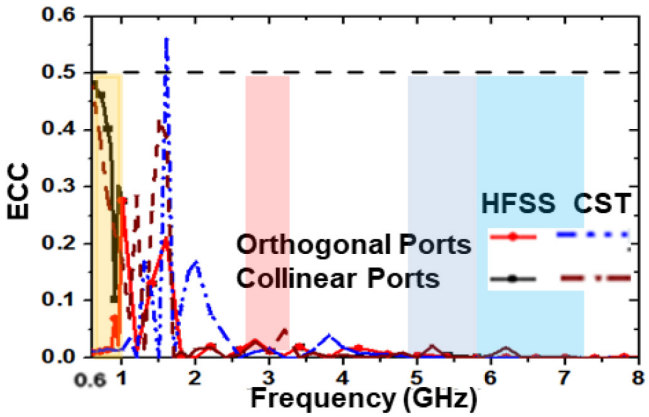

FIGURE 20. ECC comparison of CST Microwave Studio and Ansys HFSS.

B. MEAN EFFECTIVE GAIN (MEG)

The mean effective gain (MEG) is another important characteristic of the antenna which shows its suitability in multi-path environment. The MEG of the antenna has been calculated using (2) where, Γ, G_θ, and G_ϕ are the cross-

TABLE 5. Computed MEG from measured results.

Frequency (GHz)	Γ (dB)	MEG (dB)			
		Port#1	Port#2	Port#3	Port#4
0.8	0	-7.96	-7.42	-9.92	-9.53
	6	-7.79	-6.48	-9.55	-9.29
5.8	0	-6.45	-6.46	-8.55	-7.85
	6	-7.55	-6.88	-7.2	-8.91

TABLE 6. State of the art comparison of 04 port MIMO antennas.

Ref.	f_L (GHz)	Area (λ_L^2)	IBW (dB) Level	Sub-7GHz IBW (GHz)	I (dB)	Common Radiator	Co-planar Ground planar with Radiator
[8]	2.70	0.13	-10	2.7-4.94	11	No	No
[10]	3.0	0.36	-10	3.0-16.2	17.5	No	No
[11]	2.2	0.35	-10	2.2-2.5	11	No	No
[15]	2.4	0.69 2	-10	2.4-2.8 5.1-5.6	16	No	No
[16]	1.9	0.29 9	-6	1.9-3.2 3.5-3.71	15	No	No
[17]	3.5	0.29 4	-10	3.4-3.5 5.5-5.88 6.7-6.8	15	No	No
[18]	1.8	0.60 4	-10	1.8-2.9	15	Yes	No
[19]	4.4	1.21	-10	4.4-6.4	13	Yes	No
PD	**0.6**	**0.12 9**	**-6**	**0.6-1.09 2.6 -3.4 4.2-7.2**	**<1 GHz 10 dB, > 2.6 GHz 13dB**	**Yes**	**Yes**
			-10	**0.7-1.01 2.6-3.18 5.3-6.06 6.7-6.94**			

PD: Proposed design

polarization discrimination ratio, the gain pattern in θ-, and φ-planes, respectively [59]. The calculated value of MEG from the measured pattern for the different Γ is given in Table 5.

$$MEG = \frac{1}{2\pi}\int_0^{2\pi}\left[\frac{\Gamma}{1+\Gamma}G_\theta\left(\frac{\pi}{2},\phi\right) + \frac{1}{1+\Gamma}G_\phi\left(\frac{\pi}{2},\phi\right)\right]d\phi \quad (2)$$

The MEG for the outdoor and indoor environment ($\Gamma = 0$ dB and 6 dB) have been calculated. From literature, it is known that for the satisfactory performance of the MIMO antenna, the -12 dB $\leq$ MEG ≤ -3 dB is desired which has been achieved in the present case. Secondly |MEGi /MEGj| where i and j are the antenna numbers, is also less than 3 dB and thus antenna gives the satisfactory performance for the indoor as well as outdoor environment.

Although not shown here, to characterize the MIMO performance, from the measured scattering parameters, the channel capacity for a 30 dB signal to noise ratio (SNR) has also been calculated by building the channel correlation matrix elements from the S-parameters [60]–[62]. The channel capacity is 29.83 bits/sec/Hz against the ideal channel capacity of 31.88 bits/sec/Hz [60].

IX. STATE OF THE ART COMPARISON

The state of the art comparison with some recently published work is made in Table 6. At the lowest operating frequency, the antenna size outnumbers the reported structures. Further, none of the 04 port antenna dealt the sub-1GHz band, before. Due to the co-existing ground and radiating structures on the same side of the substrate, it is adaptable to the host platforms which can be advantageous for the upcoming sub-1GHz, sub-6GHz 5G NR, and the Wi-Fi 6 communication bands.

X. CONCLUSION

A four port common radiator MIMO antenna is designed to cover additional emerging communication bands above 0.6 GHz in sub-1GHz, sub-6GHz 5G NR, and the Wi-Fi 6 communication bands. A guideline to enhance the operating bandwidth and the isolation in the sub-1GHz band is presented. The antenna exhibits the pattern diversity which is useful for the MIMO applications. It can find a number of applications including Wi-Fi 6 routers, Access points, and LTE band user equipment's (UEs).

REFERENCES

[1] A. J. Paulraj, D. A. Gore, R. U. Nabar, and H. Blolcskei, "An overview of MIMO communications—A key to gigabit wireless," *Proc. IEEE*, vol. 92, no. 2, pp. 198–218, Feb. 2004.
[2] M. Sharawi, *Printed MIMO Antenna Engineering*. Boston, MA, USA: Artech House, 2014.
[3] K. R. Jha, B. Bukhari, C. Singh, G. Mishra, and S. K. Sharma, "Compact planar multistandard MIMO antenna for IoT applications," *IEEE Trans. Antennas Propag.*, vol. 66, no. 7, pp. 3327–3336, Jul. 2018.
[4] K. R. Jha and S. K. Sharma, "Combination of MIMO antennas for handheld devices," *IEEE Antennas Propag. Mag.*, vol. 60, no. 1, pp. 118–131, Feb. 2018.
[5] D. Lu, L. Wang, E. Yang, and G. Wang, "Design of high-isolation wideband dual-polarized compact MIMO antennas with multiobjective optimization," *IEEE Trans. Antennas Propag.*, vol. 66, no. 3, pp. 1522–1527, Mar. 2018.
[6] R. Anitha, P. V. Vinesh, K. C. Prakash, P. Mohanan, and K. Vasudevan, "A compact quad element slotted ground wideband antenna for MIMO applications," *IEEE Trans. Antennas Propag.*, vol. 64, no. 10, pp. 4550–4553, Oct. 2016.
[7] J. Sui, Y. Dou, X. Mei, and K.-L. Wu, "Self-curing decoupling technique for MIMO antenna arrays in mobile terminals," *IEEE Trans. Antennas Propag.*, vol. 68, no. 2, pp. 838–848, Feb. 2020.
[8] D. Sarkar and K. V. Srivastava, "A compact four-element MIMO/Diversity antenna with enhanced bandwidth," *IEEE Antennas Wireless Propag. Lett.*, vol. 16, pp. 2469–2472, 2017.
[9] C. Deng, D. Liu, and X. Lv, "Tightly arranged four-element MIMO antennas for 5G mobile terminals," *IEEE Trans. Antennas. Propag.*, vol. 67, no. 10, pp. 6353–6361, Oct. 2019.
[10] W. Wu, B. Yuan, and A. Wu, "A quad-element UWB-MIMO antenna with band-notch and reduced mutual coupling based on EBG structures," *Int. J. Antennas Propag.*, vol. 2018, Feb. 2018, Art. no. 8490740.
[11] A. T. Hassan and M. S. Sharawi, "Four element half circle shaped printed MIMO antenna," *Microw. Opt. Technol. Lett.*, vol. 58, no. 12, pp. 2990–2992, 2016.
[12] G. Wolosinski, V. Fusco, U. Naeem, and P. Rulikowski, "Pre-matched eigenmode antenna with polarization and pattern diversity," *IEEE Trans. Antennas Propag.*, vol. 67, no. 8, pp. 5145–5153, Aug. 2019.
[13] A. Ramachandran, S. Mathew, V. Rajan, and V. Kesavath, "A compact triband quad-element MIMO antenna using SRR for high isolation," *IEEE Antennas Wireless Propag. Lett.*, vol. 16, pp. 1409–1412, 2017.

[14] J.-F. Keh, M. Chou, Z.-C. Zhang, Q.-X. An, and W.-J. Liao, "A beamforming-network-based four-squint-beam array antenna for ceiling-mount access point," *IEEE Antennas Wireless Propag. Lett.*, vol. 18, no. 4, pp. 707–711, Apr. 2019.

[15] M. Ikram, N. N.-Trong, and A. Abbosh, "Multiband MIMO microwave and millimeter antenna system employing dual-function tapered slot structure," *IEEE Trans. Antennas Propag. Lett.*, vol. 67, no. 8, pp. 5705–5707, Aug. 2019.

[16] M. Ikram, M. S. Sharawi, A. Shamim, and A. Sebak, "A multiband dual-standard MIMO antenna system based on monopoles (4G) and connected slots (5G) for future smart phones," *Microw. Opt. Technol. Lett.*, vol. 60, no. 6, pp. 1468–1476, 2018.

[17] Y. Liu, M. Liu, F. Xu, J. Xu, and X. Huang, "A novel four-port high isolation MIMO antenna design for high capacity wireless applications," *Microw. Opt. Technol. Lett.*, vol. 60, no. 6, pp. 1476–1481, 2018.

[18] A. MoradiKordaliv, T. A. Rahman, and M. Khalily, "Common elements wideband MIMO antenna system for WiFi/LTE access-point applications," *IEEE Antennas Wireless Propag. Lett.*, vol. 13, pp. 1601–1604, 2014.

[19] S. Chouhan and L. Malviya, "Four-port shared rectangular radiator with defected ground for wireless application," *Int. J. Commun. Syst.*, vol. 60, no. 6, 2020, Art. no. e4356.

[20] N. Zhao and W.-P. Tian, "CPW-fed dual-band MIMO antenna with common radiating element," *Progr. Electromagn. Res. Lett.*, vol. 62, pp. 71–75, Sep. 2016.

[21] M. S. Sharawi, "Printed multi-band MIMO antenna systems and their performance metrics," *IEEE Antennas Propag. Mag.*, vol. 55, no. 5, pp. 219–232, Oct. 2013.

[22] L. Qu, H. Piao, and H. Kim, "Compact wideband MIMO mobile-antenna system design using mode-based decoupling techniques," *Int. J RF Microw. Comput. Aided Eng.*, vol.29, no. 8, 2019, Art. no. e21765.

[23] R. Luomaniemi, J.-M. Hannula, R. Kormilainen, A. Lehtovuori, and V. Viikari, "Unbroken metal rim MIMO antenna utilizing antenna clusters," *IEEE Antennas Wireless Propag. Lett.*, vol, 18, no. 6, pp. 1071–1075, Jun. 2019.

[24] *GSMA*. Accessed: Jun. 16, 2020. [Online]. Available: https://www.gsma.com/spectrum/wp-content/uploads/2020/03/5G-Spectrum-Positions.pdf

[25] A. Burger. *Nokia Claims 600 MHz LTE Equipment First—Telecompetitor*. Accessed: Jun. 16, 2020. [Online]. Available: https://www.telecompetitor.com/nokia-claims-600-mhz-lte-equipment-first/

[26] C. A. Wieczorek, "600MHz spectrum access systems and methods," U.S. Patent 10 735 969 B2, Aug. 4, 2020.

[27] S. C. D. Barrio, G. F. Pedersen, and A. S. Morris, "Tunable multiple-resonance antenna systems, devices, and methods for handsets operating in low LTE bands with wide duplex spacing," U.S. Patent 10 541 475 B2, Jan. 21, 2020.

[28] Z. M. Temeswari and D. Maros, "Data transfer rates and data traffic trends on mobile networks," *Interdiscipl. Description Complex Syst.*, vol. 17, no. 1-A, pp. 26–39, 2019.

[29] M. R. Nikkah, K. Ghaemi, and N. Behdad, "An electronically tunable biomimetic antenna array," *IEEE Trans. Antennas Propag.*, vol. 66, no. 3, pp. 1248–1257, Mar. 2018.

[30] *Global Update on Spectrum for 4G & 5G*. Accessed: Oct. 2, 2020. [Online]. Available: https://www.qualcomm.com/media/documents/files/spectrum-for-4g-and-5g.pdf

[31] L. Teschler, B. V. Says, and B. Veitch, *Test Measurement Tips: What You Should Know About Wi-Fi 6 and the 6-GHz Band*. Accessed: Jun. 20, 2020. [Online]. Available: https://www.testandmeasurementtips.com/what-you-should-know-about-wi-fi-6-and-the-6-ghz-band/

[32] RCR Wireless News and Qualcomm. (Apr. 20, 2020). *The Path Forward for Sub-7 GHz Wide-Area 5G Technology*. Accessed: Jun. 16, 2020. [Online]. Available: https://www.rcrwireless.com/20200402/5g/the-path-forward-for-sub-7-ghz-wide-area-5g-technology

[33] C. Chen, J. Li, V. Balasubramaniam, Y. Wu, Y. Zhang, and S.Wan, "Contention resolution in Wi-Fi 6 enabled Internet of Things based on deep learning," *IEEE Internet of Things J.*, vol. 8, no. 7, pp. 5309–5320, Apr. 2021, doi: 10.1109/JIOT.2020.3037774.

[34] G. Naik, J.-M. Park, J. Ashdown, and W. Lehr, "Next generation Wi-Fi and 5G NR-U in the 6 GHz bands: Opportunities and challenges," *IEEE Access*, vol. 8, pp. 153027–153056, 2020.

[35] V. Maglogiannis, A. Shahid, D. Naudts, E. D. Poorter, and I. Moerman, "Enhancing the coexistence of LTE and Wi-Fi in unlicensed spectrum through convolutional neural networks," *IEEE Access*, vol. 7, pp. 28464–28477, 2019.

[36] J. Liang, C. C. Chiau, X. Chen, and C. G. Parini, "Printed circular disc monopole antenna for ultra-wideband applications," *Electron. Lett.*, vol. 40, no. 20, pp. 1246–1247, 2004.

[37] J. Liang, C. C. Chiau, X. Chen, and C. G. Parini, "Study of a printed circular disc monopole antenna for UWB systems," *IEEE Trans. Antennas Propag.*, vol. 53, no. 11, pp. 3500–3504, Nov. 2005.

[38] K. P. Ray and Y. Ranga, "Ultrawideband printed elliptical monopole antennas," *IEEE Trans. Antennas propag.*, vol. 55, no. 4, pp. 1189–1192, Apr. 2007.

[39] W. Jiang, Y. Liu, S. Gong, and T. Hong, "Application of bionics in antenna radar cross section reduction," *IEEE Antennas Wireless Propag. Lett.*, vol. 8, pp. 1275–1278, 2009.

[40] K. Zhang, Y. Li, and Y. Long, "Band-notched UWB printed monopole antenna with a novel segmented circular patch," *IEEE Antennas Wireless Propag. Lett.*, vol. 9, pp. 1209–1212, 2010.

[41] W.-C. Liu, C.-M. Wu, and Y.-J. Tseng, "Parasitically loaded CPW-fed monopole antenna for broadband operation," *IEEE Trans. Antennas Propag.*, vol. 59, no. 6, pp. 2415–2419, Jun. 2011.

[42] M. N. Srifi, S. K. Podilchak, M. Essaaidi, and Y. M. M. Antar, "Compact disc monopole antennas for current and future ultrawideband (UWB) applications," *IEEE Trans. Antennas. Propag.*, vol. 59, no. 12, pp. 4470–4480, Dec. 2011.

[43] M. Shokri, H. Shirzad, S. Movagharnia, B. Virdee, Z. Amiri, and S. Asiaban, "Planar monopole antenna with dual interference suppression functionality," *IEEE Antennas Wireless Propag. Lett.*, vol. 12, pp. 1554–1557, 2013.

[44] J. Y. Siddiqui, C. Saha, and Y. M. M. Antar, "Compact SRR loaded UWB circular monopole antenna with frequency notch characteristics," *IEEE Trans. Antennas Propag.*, vol. 62, no. 8, pp. 4015–4020, Aug. 2014.

[45] J. Y. Siddiqui, C. Saha, and Y. M. M. Antar, "Compact dual-SRR-loaded UWB monopole antenna with dual frequency and wideband notch characteristics," *IEEE Antennas Wireless Propag. Lett.*, vol. 14, pp. 100–103, 2015.

[46] P.-Y. Qin, F. Wei, and Y. J. Guo, "A wideband-to-narrowband tunable antenna using a reconfigurable filter," *IEEE Trans. Antennas Propag.*, vol. 63, no. 5, pp. 2282–2285, May 2015.

[47] X.-W. Dai, T. Zhou, and G.-F. Cui, "Dual-band microstrip circular patch antenna with monopolar radiation pattern," *IEEE Antennas Wireless Propag. Lett.*, vol. 15, pp. 1004–1007, 2016.

[48] H. Tang, K. Wang, R. Wu, C. Yu, J. Zhang, and X. Wang, "Novel broadband circularly polarized monopole antenna based on C-shaped radiator," *IEEE Antennas Wireless Propag. Lett.*, vol. 16, pp. 964–967, 2017.

[49] T. K. Saha, C. Goodbody, T. Karacolak, and P. K. Sekhar, "A compact monopole antenna for ultra-wideband applications," *Microw. Opt. Technol. Lett.*, vol. 61, no. 1, pp. 182–186, 2019.

[50] S. Kundu, "Experimental study of a printed ultra-wideband modified circular monopole antenna," *Microw. Opt. Technol. Lett.*, vol. 61, no. 1, pp. 1–6, 2019.

[51] M. A. Antoniades and G. V. Eleftheriades, "A compact multiband monopole antenna with a defected ground plane," *IEEE Antennas Wireless Propag. Lett.*, vol. 7, pp. 652–655, 2008.

[52] A. Kumar, J. K. Deegwal, and M. M. Sharma, "Design of multi-polarized quad-band planar antenna with parasitic multistubs for multiband wireless communication," *IET Microw. Antennas Propag.*, vol. 12, no. 5, pp. 718–726, 2018.

[53] B. K. Lau, D. Manteuffel, H. Arai, and S. V. Hum, "Guest editorial theory and applications of characteristic modes," *IEEE Trans. Antennas Propag.*, vol. 64, no. 7, pp. 2590–2595, Jul. 2016.

[54] Q. Wu, "General metallic-dielectric structures: A characteristic mode analysis using volume surface formulations," *IEEE Antennas Propag. Mag.*, vol. 61, no. 3, pp. 27–36, Jun. 2019.

[55] C. Wang, Y. Chen, and S. Yang, "Bandwidth enhancement of a dual-polarized slot antenna using characteristic modes," *IEEE Antennas Wireless Propag. Lett.*, vol. 17, no. 6, pp. 988–992, Jun. 2018.

[56] X. Yang, Y. Liu, and S.-X. Gong, "Design of a wideband omnidirectional antenna with characteristic mode analysis," *IEEE Antennas Wireless Propag. Lett.*, vol. 17, no. 6, pp. 993–997, Jun. 2018.

[57] G. Kumar and K. P. Ray, *Broadband Microstrip Antennas*. Boston, MA, USA: Artech House, 2003.
[58] K. R. Jha and S. K. Sharma, "A novel four-port pattern diversity antenna for 4G communications," in *Proc. IEEE Int. Symp. Antennas Propag.*, Jul. 2018, pp. 27–28.
[59] Z. Chen, W. Geyi, M. Zhang, and J. Wang, "A study of antenna system for high order MIMO device," *Int. J. Antennas Propag.*, vol. 2016, Mar. 2016, Art. no. 1936797.
[60] Y. Zhang, J.-Y. Deng, M.-J. Li, D. Sun, and L.-X. Guo, "A MIMO dielectric resonator antenna with improved isolation for 5G mm-Wave applications," *IEEE Antennas Wireless Propag. Lett.*, vol. 18, no. 4, pp. 747–751, Apr. 2019.
[61] J. Thaysen and K. B. Jakobsen, "Envelope correlation in (N,N) MIMO antenna array from scattering parameters," *Microw. Opt. Technol. Lett.*, vol. 48, no. 5, pp. 832–834, 2006.
[62] Y. K. Choukiker, S. K. Sharma, and S. K. Behra, "Hybrid fractal shape planar monopole antenna covering multiband wireless communications with MIMO implementation for handheld devices," *IEEE Trans. Antennas Propag.*, vol. 62, no. 3, pp. 1483–1488, Mar. 2014.

KUMUD RANJAN JHA (Senior Member, IEEE) received the bachelor's degree from the Institution of Engineers, India, in 1999, the master's degree in electronics and communication engineering (ECE) from the Birla Institute of Technology, Ranchi, India, in 2007, and the Ph.D. degree in ECE from the Jaypee University of Information Technology, Waknaghat, India, in 2012.

In 2007, he joined Shri Mata Vaishno Devi University, Katra, India, as an Assistant Professor, where he is currently an Associate Professor. Prior to joining academia, he served in the Indian Air Force for more than a decade. He is a Postdoctoral Fellow with San Diego University, San Diego, CA, USA. He has authored over 85 articles in journals and conferences and coauthored the book *Terahertz Planar Antennas for Next Generation Communication*. He is also credited with book chapters in *Multifunctional Antennas and Arrays for Wireless Communication Systems* (IEEE Press/Wiley, USA, 2021). His current research interests include microwave/RF passive/active component design and terahertz electronics for future wireless communication. He is the recipient of the 2012 Raman Fellowship Awarded by the University Grant Commission, Government of India, for the postdoctoral study in the USA.

Z. A. PANDIT JIBRAN was born in Jammu and Kashmir, India, in 1995. received the bachelor's degree from the Islamic University of Science and Technology in 2018, and the master's degree in electronics and communication engineering from Shri Mata Vaishno Devi University, India, in 2020. He has completed his major and minor projects in the Microwave and Antenna domain. He is currently a RF and Microwave Design Engineer with RFMW Innovations Lab Private Ltd., Bengaluru, India. His research interests include active and passive frequency selective surfaces, absorbers, MIMO antennas, and wearable antenna design for the body centric applications.

CHITRA SINGH (Member, IEEE) received the B.Tech. and M.Tech. degrees in electronics and communication engineering from G.B.P.U.A.&T., Pantnagar, India, in 2005 and 2009, respectively, and the Ph.D. degree in electronics and communication engineering from Shri Mata Vaishno Devi University, Katra, India, in 2019.

She is currently working as an Assistant Professor with the Center for Advanced Studies, Dr. A. P. J. Abdul Kalam Technical University, Lucknow, India. She has coauthored over 25 papers in international journals and conferences. Her current research interests include the analysis and design of frequency selective structures, absorbers, filters, microstrip antennas, and numerical techniques for modeling RF/microwave components and antennas. She is the recipient of the Teaching Assistantship from MHRD, India, during her studies.

SATISH KUMAR SHARMA (Senior Member, IEEE) received the B.Tech. degree in electronics engineering from the Kamla Nehru Institute of Technology in 1991, and the Ph.D. degree in electronics engineering from the Indian Institute of Technology, Banaras Hindu University in 1997.

From March 1999 to April 2001, he was a Postdoctoral Fellow with the Department of Electrical and Computer Engineering, University of Manitoba, Winnipeg, MB, Canada. He was a Senior Antenna Engineer with InfoMagnetics Technologies Corporation, Winnipeg, from May 2001 to August 2006. He was also a Research Associate with the University of Manitoba from June 2001 to August 2006. In August 2006, he joined San Diego State University, San Diego, as an Assistant Professor with the Department of Electrical and Computer Engineering, where he has developed an Antenna Laboratory, teaches courses in applied electromagnetics, and advises B.S., M.S., and Ph.D. students and postdoctoral fellows. Since 2014, he has been a Full Professor and the Director of the Antenna and Microwave Laboratory. His research lab consists of both far-field anechoic chamber (800MHz–40GHz) and mini-compact antenna test range (M-CATR: 26.50GHz–110GHz) for antenna radiation pattern characterization in addition to other instrumentation and simulation tools. He has authored/coauthored of more than 270 research papers published in the referenced international journals and conferences. He has co-edited three volumes of *Handbook of Reflector Antennas and Feed Systems, Volume 1: Theory and Design of Reflectors, Volume II: Feed Systems, and Volume III: Applications of Reflectors* (Artech House, USA). His new coedited/coauthored book *Multifunctional Antennas and Arrays for Wireless Communication Systems* (IEEE Press/Wiley, USA, April 2021). He holds one U.S. and one Canadian patents. His main research interests are in the millimeter wave antennas, active phased array antennas, massive MIMO antennas, 5G communication antennas, antennas for IoT, GPS, handheld and portable devices, reconfigurable and frequency agile antennas, null-steering antennas, feeds for reflector antennas, waveguide horns and polarizers, miniaturized antennas for body wearable applications, 3D printed antennas, frequency selective surfaces, metasurfaces, and microwave passive components such as phase shifters, power dividers and beam forming networks using 5G silicon RFICs.

Dr. Sharma received the IEEE AP-S Harold A. Wheeler Prize Paper Award in 2015, the National Science Foundation's Prestigious Faculty Early Development (CAREER) Award in 2009, the Young Scientist Award of URSI Commission B, Field and Waves, during the URSI Triennial International Symposium on Electromagnetic Theory, Pisa, Italy, in 2004. He was the Chair/Co-Chair of the several Student Paper Contests in different conferences and symposia and served on the sub-committee of the Education Committee for the IEEE Antennas and Propagation Society for the organization of the Student Paper Contests. He was recognized as the Outstanding Associate Editor (AE) for the IEEE TRANSACTIONS ON ANTENNAS AND PROPAGATION in July 2014. He served as the AE for the IEEE TRANSACTIONS ON ANTENNAS AND PROPAGATION. He is currently serving as the AE for the IEEE ANTENNAS AND WIRELESS PROPAGATION LETTERS and he is on the editorial board of *International Journal of RF and Microwave Computer-Aided Engineering*. He is a Full Member of the USNC/URSI, Commission B, a Senior Member of URSI, and currently serving as the Chair of Technical Activities for the USNC/URSI Commission B.